Thermal Effects and Vibrational Corrections to Transition Metal NMR Chemical Shifts

Sonja Grigoleit and Michael Bühl*[a]

Dedicated to Professor Wolfgang von Philipsborn on the occasion of his 75th birthday

Abstract: Both zero-point and classical thermal effects on the chemical shift of transition metals have been calculated at appropriate levels of density functional theory for a number of complexes of titanium, vanadium, manganese and iron. The zero-point effects were computed by applying a perturbational approach, whereas classical thermal effects were probed by Car–Parrinello molecular dynamics simulations. The systematic investigation shows that both procedures lead to a deshielding of the magnetic shielding constants evaluated at the GIAO-B3LYP level, which in general also leads to a downfield shift in the relative chemical shifts, δ. The effect is small for the titanium and vanadium complexes, where it is typically on the order of a few dozen ppm, and is larger for the manganese and iron complexes, where it can amount to several hundred ppm. Zero-point corrections are usually smaller than the classical thermal effect. The pronounced downfield shift is due to the sensitivity of the shielding of the metal centre with regard to the metal–ligand bond length, which increase upon vibrational averaging. Both applied methods improve the accuracy of the chemical shifts in some cases, but not in general.

Keywords: density functional calculations · molecular dynamics · NMR spectroscopy · transition metals

Introduction

NMR spectroscopy is one of the most important methods for the characterization of electronic and structural properties of molecules.[1] This is particularly true for the lighter nuclei such as ^{1}H or ^{13}C, but due to improved techniques the NMR chemical shifts of formerly "exotic" nuclei such as transition metals[2,3] are becoming more and more accessible. The possibility to probe with NMR the very centre of a transition-metal complex has opened many fruitful applications for this important class of compounds.[4]

Whereas density functional theory (DFT) has been the workhorse for computational transition-metal chemistry for some time,[5] it was not until the mid-nineties that DFT calculations could be performed which describe the chemical shifts of transition-metal nuclei properly.[6–9] It has turned out that the quantum chemical investigation of transition-metal nuclei is quite elaborate and far from being a black-box method. For instance it has been shown that the metal chemical shifts can depend strongly on the density functionals used.[8,10,11] A combination of functionals, B3LYP for BP86 optimized geometries, turned out to be optimal for the overwhelming majority of cases studied so far. The calculations were performed for static equilibrium geometries, that is, for vibrationless molecules at a temperature of 0 K. Present methodological developments are aimed at taking the actual experimental conditions into account. The first way to assess the thermal effects on the transition metal chemical shifts was based on Car–Parrinello molecular dynamics (CPMD) simulations.[12] For the determination of the thermally averaged chemical shift, a number of snapshots were collected along the trajectory over a period of a few ps, and for each snapshot the chemical shift was computed at the appropriate DFT level. This approach, pioneered by Huber et al.[13] on the basis of classical MD simulations for the gas-to-liquid shifts in water, was subsequently applied to a number of transition-metal complexes,[14–16] usually in aqueous solution.

Since these simulations are based on classical molecular dynamics propagation, zero-point effects, which are purely quantum mechanical in nature, are not included. For small molecules, such effects can be accounted for by full or partial solutions of the nuclear Schrödinger equation.[17] For medium sized molecules, effects of quantum fluctuations on

[a] Dr. S. Grigoleit, Dr. M. Bühl
Max-Planck Institut für Kohlenforschung
Kaiser-Wilhelm-Platz 1
45470 Mülheim an der Ruhr (Germany)
Fax: (+49) 208-306-2996
E-mail: buehl@mpi-muelheim.mpg.de

Supporting information for this article is available on the WWW under http://www.chemeurj.org/ or from the author.

 DOI: 10.1002/chem.200400256

chemical shifts can be assessed by suitable quantum Monte Carlo methods.[18] More approximate, but general methods have been devised to assess the effect of vibrational and zero-point corrections on molecular properties of larger molecules.[19–21] Of these perturbational approaches, we employed that proposed by Ruud et al. in which the anharmonic contribution of the potential is used to shift the molecule from the equilibrium geometry to an effective geometry, which is equivalent to the vibrationally averaged structure.[22–24] The magnetic shielding hypersurface is expanded around this effective geometry, so that the procedure yields a vibrationally averaged magnetic shielding. For small molecules it was shown that the zero-point correction of the chemical shift could be as large as the effect of electron correlation.[22] Reliable results were reported for ^{1}H[22] and ^{19}F[25] chemical shifts.

We have recently applied this approach to compute the vibrationally corrected magnetic shielding constants of three transition-metal complexes: $[VOCl_3]$, $[MnO_4]^-$, and $[Fe(CO)_5]$.[26] No direct comparison with experimental data was possible, and it was concluded that relative chemical shifts of a larger set of compounds should be studied.

We now report such a systematic, comprehensive investigation of the performance of these methods for transition-metal shifts of selected test sets comprising Ti, V, Mn and Fe complexes. These test sets cover large parts of the total chemical shift ranges of these nuclei, namely about 2700, 3500, 3800, and 2100 ppm for ^{49}Ti, ^{51}V, ^{55}Mn and ^{57}Fe, respectively.[27] The complexes of the test sets have been used previously for assessment of static chemical-shift calculations.[11,28–30] Zero-point corrected Ti chemical shifts have been reported before;[28] we now include the classical, CPMD derived thermal effects for comparison. Thus, we use two different approaches to go beyond static equilibrium values for the computed chemical shifts: On the one hand we investigate the effect of the temperature on the magnetic shielding employing the CPMD based approach, where the movement of the molecule on the (quantum chemical calculated) potential surface is determined by classical mechanical laws. The influence of the zero-point vibration on the magnetic shielding, on the other hand, is estimated with a quantum mechanical treatment that takes the anharmonicity of the potential energy surface into account. Objective of the present study is to determine whether these methods would lead to a systematic improvement of the theoretical transition metal chemical shifts over those obtained from conventional static calculations. As it turns out, neither method produces such a systematic increase in accuracy, even though the description of individual systems can be markedly improved.

Computational Methods

Geometries have been fully optimized employing the gradient-corrected exchange-correlation functionals of Becke[31] and Perdew,[32,33] denoted BP86, together with a fine integration grid (75 radial shells with 302 angular points per shell). For the optimization we employed basis AE1, that is, Wachters' all-electron basis augmented with one additional diffuse d and two p functions with the contraction Scheme (14s11p6d)/[8s7p4d] for the transition metals Ti, Mn, V, and Fe,[34,35] and 6-31G* basis for all other elements. All structures were characterized as minima on the potential energy surface by the absence of imaginary harmonic vibrational frequencies. The stationary DFT geometries were taken from earlier studies[11,28–30] and, for the zero-point corrections, reoptimized to gradients better than 1.0×10^{-5} a.u.

To check if the 6-31G* basis of the ligands is sufficient to compute molecular properties which depend on the curvature of the potential energy surface (PES), we compared the calculated harmonic frequencies with the experimental fundamentals (see Figure 1 and Table S1–S4 of the Supporting Information). For this purpose we chose one representative compound out of each group of the Ti, V, Mn and Fe complexes; namely $[TiCl_3Me]$,[36] $[VO(OCH_2CH_2O)_3N]$,[37] $[Mn(CO)_5H]$[38,39] and $[FeCp_2]$.[40,41] Note that these compounds contain hydrogen atoms, which in the 6-31G* basis carry no polarization functions; therefore basis set deficiencies should be most pronounced in these compounds. For all strong and very strong, unambiguously assigned bands, the calculated and experimental frequencies agree very well, with the slope of the correlation close to unity.[42] Thus, the usage of the medium-sized 6-31G* basis is well justified and appears to be sufficient for a proper description of the relevant parts of the PES.

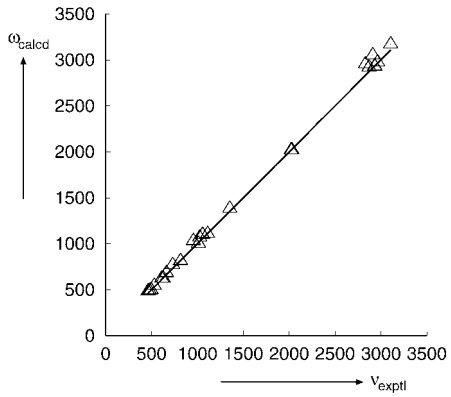

Figure 1. Plot of the calculated harmonic frequencies of $[TiCl_3Me]$, $[VO(OCH_2CH_2)_3N]$, $[Mn(CO)_5H]$ and $[FeCp_2]$ versus the experimental IR frequencies; only the strong and very strong fundamentals were used (slope of the correlation line: 1.015, correlation coefficient 0.999).

Magnetic shielding tensors have been computed with the gauge-including atomic orbitals method (GIAO) as implemented[43] in the Gaussian98 program,[44] employing the B3LYP hybrid functional[45,46] and Basis II', that is, the same augmented Wachters basis set for the transition metals and the IGLO-II basis[47] for the ligands except H: a (9s5p)/[5s4p] basis augmented with one set of d-polarization functions for C, N, O, F, a (11s7p)/[7s6p] basis with two sets of d-polarization functions for Al, Si, Cl, and a (3s)/[2s] basis for H.

Molecular dynamics simulations were performed by using the density-functional based Car–Parrinello scheme[12] as implemented in the CPMD program.[48] The BP86 functional was used, together with norm-conserving Troulier–Martins pseudopotentials in the Kleinman–Bylander form.[49,50] Periodic boundary conditions were imposed by using supercells with box sizes between 11.5 and 14 Å so that the minimum distance between atoms in neighbouring virtual boxes is larger than 5.8 Å. Kohn–Sham orbitals were expanded in plane waves up to a kinetic energy cutoff of 80 Ry. In the dynamic simulations a fictitious electronic mass of 600 a.u. and a time step of 0.121 fs were used. From the microcanonical runs with an average temperature of 300 K snapshots were collected for the NMR calculations: after an equilibration time of 0.5 ps, 41 snapshots were taken every 24 fs (total time ca. 1 ps). Equilibrium geometries for the compounds were obtained by optimizing the forces on all atoms with the CPMD program using the set-up detailed above (denoted CP-Opt);

additionally the averaged structural parameters were computed from the microcanonical run (denoted CPMD).

Vibrational corrections were computed by using the perturbational approach of Ruud et al.[22–24] In this method, the molecule is first shifted from its equilibrium geometry r_e to an effective geometry r_{eff} via the harmonic frequencies ω_e and the cubic force field $V^{(3)}$ as in Equation (1):

$$r_{eff,j} = r_{e,j} - \frac{1}{4\omega_{e,j}^2} \sum_m \frac{V^{(3)}_{e,jmm}}{\omega_{e,m}} \quad (1)$$

This effective geometry corresponds to the vibrationally averaged structure of a system at 0 K. Due to the anharmonicity of the PES the effective bond lengths are typically slightly longer than the equilibrium ones. Second, the magnetic shielding tensor is expanded in a Taylor series around this effective geometry. Thus, the expansion term containing the perturbed vibrational wavefunction to first order vanishes and for the computation of the magnetic shielding to second order only the zeroth order vibrational wave function is needed. The equation for the calculation of the vibrationally averaged magnetic shielding is thus simplified to Equation (2):

$$\sigma_0 = \sigma_{eff} + \frac{1}{4} \sum_i \frac{\sigma^{(2)}_{eff,ii}}{\omega_{eff,i}} \quad (2)$$

where $\sigma^{(2)}_{eff}$ is the second derivative of the magnetic shieding, evaluated numerically, and σ_{eff} and ω_{eff} are magnetic shielding constant and the harmonic frequencies, both computed at the effective geometry.

In essence the vibrationally averaged magnetic shielding includes the leading contributions from both the anharmonicity of the PES (through the use of the effective geometry as an expansion point) and from the curvature of the magnetic shielding hypersurface.

For the computation of r_{eff} and σ_0 the corresponding parts of the Dalton program package[51] had been adapted so that energies, energy derivatives and properties produced with Gaussian98 can be processed.[26] $V^{(3)}$ is obtained numerically at the BP86/AE1 level using the gradient technique, and a stepsize of 0.25 a.u. for the finite displacements, as recommended by the test calculations in an earlier study.[26] For the computation of $\sigma^{(2)}_{eff}$ we used a stepsize of 0.1 a.u. as recommended by the test calculations in the same study.[26]

To compute the effective geometries of $[VO(CH_3)_3]$, $[VO(CH_3)_3AlH_3]$, and $TiMe_4$ with sufficent numerical precision, it was necessary to employ an ultrafine integration grid (99 radial shells with 590 angular points per shell). In these cases, the error-prone low-frequency modes of -CH_3 rotations lead to abnormal, long C–H bond lengths (>1.2 Å). Ruud et al.[22] reported that for some molecules imaginary frequencies are obtained, which are associated with internal rotations. It was argued that these modes can be decoupled from the other modes in a "Born–Oppenheimer-type approximation" and the neglect of these imaginary modes was justified by demonstrating that these modes do not contribute significantly to the zero-point correction. Following this arguments we neglect this internal rotation in the calculation of the zero-point effect, when it leads to obvious artifacts in the effective geometry. No such artifacts were encountered in the remaining molecules of the present study. Absolute magnetic shielding constants for the standard molecules, obtained with the approaches described above, are collected in Table 1.

Table 1. Equilibrium (σ_e), effective (σ_{eff}), zero-point corrected (σ_0) and averaged (σ_{av}) magnetic shieldings of the reference compounds [ppm].[a]

	σ_e(G98)	σ_{eff}	σ_0	σ_e(CP-opt)	σ_{av}(CPMD)
$[TiCl_4]$	−1025	−1032	−1033	−1017	−1034
$[VOCl_3]$	−2306	−2323	−2325	−2264	−2292
$[MnO_4]^-$	−4832	−4892	−4896	−4794	−4829
$[Fe(CO)_5]$	−2914	−2996	−3012	−2919	−3188

[a] Values for $[VOCl_3]$, $[MnO_4]^-$ and $[Fe(CO)_5]$ from ref. [26], values for $TiCl_4$ from ref. [38].

Results

Geometries: The test sets of this study, comprising most or all of these of the previous surveys of theoretical Ti,[28] V,[11] Mn[29] and Fe[30] chemical shifts are depicted in Figure 2.

The important geometrical parameters of these complexes, optimized or simulated by using the BP86 functional, are collected in Tables 2–5, together with corresponding

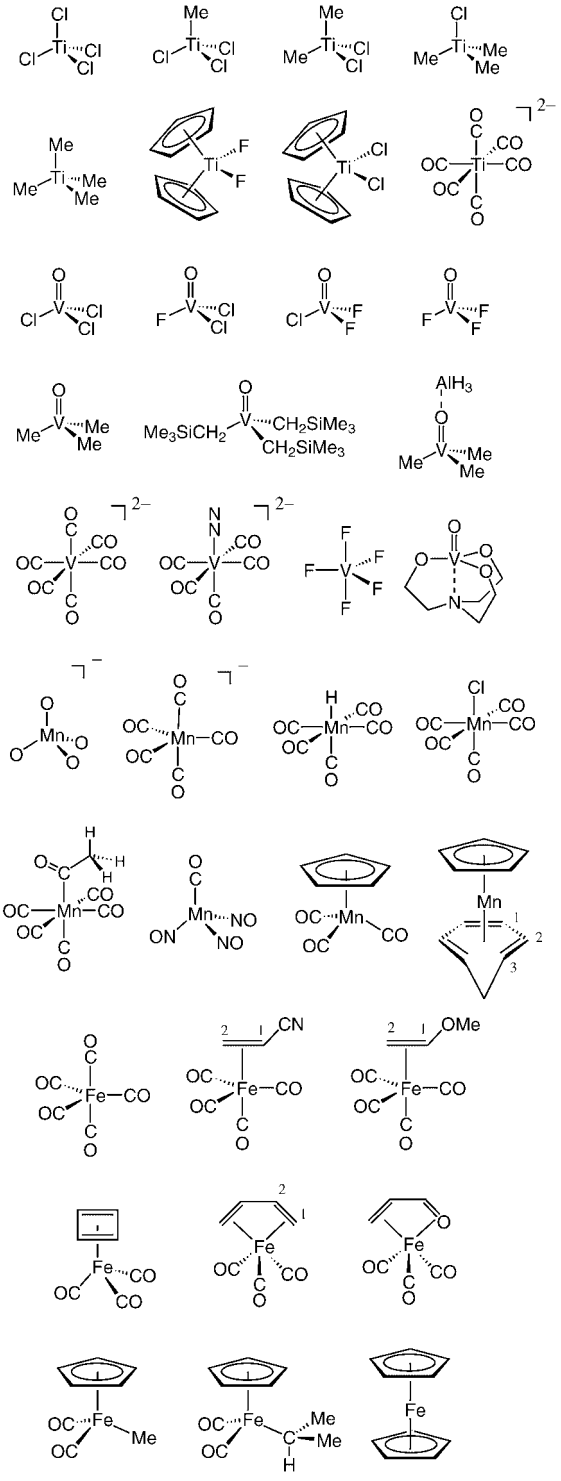

Figure 2. Ti, V, Mn and Fe complexes of this study.

Table 2. Equilibrium (r_e), effective (r_{eff}), and averaged (r_{av}) geometrical parameters for Ti complexes [Å]; for simplicity the averaged bond lengths are given where appropriate.

		r_e(G98)[a]	r_{eff}[a]	r_e(CP-opt)	r_{av}(CPMD)	exptl
$[TiCl_4]$	Ti–Cl	2.191	2.194	2.188	2.194	2.170(2)[52]
$[TiCl_3Me]$	Ti–Cl	2.204	2.207	2.197	2.206	2.185(3)[53]
	Ti–C	2.043	2.043	2.042	2.052	2.047(6)[53]
$[TiCl_2Me_2]$	Ti–Cl	2.219	2.223	2.210	2.218	2.196(3)[54]
	Ti–C	2.055	2.055	2.053	2.065	2.058(4)[54]
$[TiClMe_3]$	Ti–Cl	2.236	2.241	2.224	2.233	
	Ti–C	2.069	2.068	2.068	2.072	
$[TiMe_4]$	Ti–C	2.085	2.084	2.082	2.086	
$[TiCp_2F_2]$	Ti–C	2.446	2.460	2.431	2.469	
	Ti–F	1.835	1.836	1.846	1.845	
$[TiCp_2Cl_2]$	Ti–C	2.428	2.442	2.421	2.450	2.34–2.40[63,64]
	Ti–Cl	2.354	2.354	2.336	2.345	2.364(3)[63,64]
$[Ti(CO)_6]^{2-}$	Ti–C	2.060	2.066	2.059	2.058	2.038(3)[65]

[a] From ref. [28].

Table 3. Equilibrium (r_e), effective (r_{eff}), and averaged (r_{av}) geometrical parameters for V complexes [Å]; for simplicity the averaged bond lengths are given where appropriate.

		r_e(G98)	r_{eff}	r_e(CP-opt)	r_{av}(CPMD)	exptl
$[V(CO)_6]^-$	V–C	1.963	1.969	1.951	1.958	1.933(7)[69]
$[V(CO)_5N_2]^-$	V–C_{ax}	1.940	1.946	1.926	1.939	
	V–C_{eq}	1.965	1.971	1.953	1.964	
	V–N	2.008	2.017	1.983	1.999	
$[VF_5]$	V–F_{ax}	1.768	1.770	1.756	1.760	1.734(7)[58]
	V–F_{eq}	1.730	1.734	1.709	1.718	1.708(5)[58]
$[VOF_3]$	V–O	1.584	1.586	1.581	1.582	1.570(5)[57]
	V–F	1.737	1.740	1.722	1.727	1.729(2)[57]
$[VOClF_2]$	V–O	1.582	1.584	1.579	1.581	
	V–Cl	2.164	2.168	2.149	2.155	
	V–F	1.736	1.738	1.721	1.726	
$[VO(OCH_2CH_2)_3N]$	V–O	1.604	1.604	1.597	1.598	1.633(6)[37]
	V–O_{cyc}	1.826	1.830	1.824	1.826	1.794(4)[37]
	V···N	2.492	2.503	2.465	2.487	2.276(7)[37]
$[VOCl_2F]$	V–O	1.581	1.582	1.579	1.580	
	V–F	1.735	1.737	1.720	1.729	
	V–Cl	2.161	2.165	2.146	2.153	
$[VOCl_3]$[a]	V–O	1.579	1.580	1.579	1.579	1.570(5)[55,56]
	V–Cl	2.159	2.162	2.145	2.149	2.142(2)[55,56]
$[VO(CH_3)_3]$	V–O	1.591	1.593	1.583	1.586	
	V–C	2.028	2.030	2.019	2.026	
$[VO(CH_2Si(CH_3)_3)_3]$	V–O	1.602	–	1.595	1.590	
	V–C	2.016	–	2.006	2.016	
$[VO(CH_3)_3AlH_3]$	V–O	1.629	1.631	1.615	1.628	
	V–C	2.009	2.008	1.996	2.010	

[a] From ref. [26].

data observed in the gas phase[37,52–62] or in the solid state.[63–69] The tables include the equilibrium bond lengths computed with both Gaussian98 and the CPMD program, as well as zero-point corrected and thermal averaged bond lengths. The structural data are in good accord with the experimental gas-phase data. The deviation is around 0.5–2 pm for the gas-phase data and 1–3.5 pm for the experimental crystal structures, where the calculated bond lengths tend to be overestimated. As expected, both methods—thermal averaging and zero-point correction—show the same qualitative effect, they both lead to bond elongation. While the average elongation of the metal-ligand bonds due to the thermal averaging amounts to 1.0, 0.7, 1.4, and 2.0 pm for the Ti, V, Mn and Fe complexes, respectively, the elongation due to the zero-point correction is considerably smaller (0.4, 0.3, 0.6, and 0.8 pm for the Ti, V, Mn and Fe complexes, respectively).

For some Ti–C(H_3) bonds a slight *decrease* in the r_{eff} values with respect to r_e is predicted (by 0.001 Å or less, compare Table 2). It is not clear at this point if this effect is real or an artifact of insufficient precision in the numerical differentiation and integration procedures. Likewise, the Ti–C(O) bond in $[Ti(CO)_6]^{2-}$, averaged over the CPMD trajectory, is slightly shorter than in the equilibrium geometry (by 0.001 Å, Table 2). Closer inspection of the trajectory reveals that this bond contraction is localized on two Ti–C bonds trans to each other and that the molecular motion during the simulation time resembles that of an umbrella type bending of the four equatorial CO ligands along this axis.[70] Apparently, only one of these triply degenerate modes is followed over the course of 1 ps. Arguably, significantly longer simulation times would be needed for a properly equilibrated distribution of the kinetic energy over all vibrational degrees of freedom. Since all of these computed bond contractions are very small and barely significant, we will not discuss them further.

The compounds $[VOMe_3]$ and $[VOMe_3AlH_3]$ represent model compounds for the bulkier derivatives $[VO(CH_2SiMe_3)_3]$ and $[VO(CH_2SiMe_3)_3Al(CH_2SiMe_3)_3]$, which have been studied in context with olefin polymerisation.[11] To justify the use of model compounds we have investigated both $[VO(CH_2SiMe_3)_3]$ as well as its model compound $[VOMe_3]$. To determine the global minimum of the $[VO(CH_2SiMe_3)_3]$ molecule we have carried out a conformation analysis. We found four minima on the potential energy surface, which differ in the dihedral angles d(OVCSi). The conformer with the lowest energy has C_3 symmetry and three dihedral angles of 38.8° (Figure 3). The other conformers, where one or more trimethylsilyl groups are bent away from the oxo ligand (d(OVCSi) ≈70–80°), are only 4–7 kJ mol^{-1} higher in energy. We performed CP-molecular dynamics calculations starting from the conformer with the lowest energy, which remained stable (i.e., did not rearrange to another conformation) for the total

Table 4. Equilibrium (r_e), effective (r_{eff}), and averaged (r_{av}) geometrical parameters for Mn complexes [Å]; for simplicity the averaged bond lengths are given where appropriate.

		r_e(G98)	r_{eff}	r_e(CP-opt)	r_{av}(CPMD)	exptl
$[Mn(CO)_5]^-$	Mn–C_{ax}	1.833	1.837	1.833	1.842	1.820(11)[66]
	Mn–C_{eq}	1.814	1.818	1.809	1.818	1.798(12)[66]
$[Mn(CO)_5H]$	Mn–H	1.578	1.593	1.578	1.581	1.601(16)[59]
	Mn–C_{ax}	1.851	1.857	1.856	1.864	1.822(12)[59]
	Mn–C_{eq}	1.851	1.855	1.851	1.860	1.853(13)[59]
$[MnCp(CO)_3]$	Mn–C(Cp)	2.168	2.175	2.186	2.203	2.138(3)[67]
	Mn–C(CO)	1.795	1.801	1.784	1.792	1.793(3)[67]
$[Mn(CO)_5(COMe)]$	Mn–C	2.203	2.211	2.197	2.249	
	Mn–C_{ax}(CO)	1.847	1.853	1.844	1.857	
	Mn–C_{eq}(CO)	1.856	1.862	1.857	1.865	
$[Mn(NO)_3(CO)]$	Mn–N	1.699	1.702	1.698	1.703	
	Mn–C	1.861	1.867	1.862	1.875	
$[Mn(CO)_5Cl]$	Mn–Cl	2.399	2.403	2.399	2.414	2.367(4)[68]
	Mn–C_{ax}	1.818	1.824	1.809	1.819	1.807(9)[68]
	Mn–C_{eq}	1.872	1.879	1.872	1.884	1.893(6)[68]
$[MnO_4]^-$[a]	Mn–O	1.625	1.628	1.622	1.624	1.629 ± 0.005[83]
$[MnCp(C_7H_8)]$[b]	Mn–C(Cp)	2.121	2.129	2.120	2.142	
	Mn–C^1	2.116	2.123	2.116	2.129	
	Mn–C^2	2.102	2.109	2.099	2.111	
	Mn–C^3	2.168	2.177	2.166	2.187	

[a] From ref. [26]. [b] See Figure 2 for numbering.

Table 5. Equilibrium (r_e), effective (r_{eff}), and averaged (r_{av}) geometrical parameters for Fe complexes [in Å]; for simplicity the averaged bond lengths are given where appropriate.

		r_e(G98)	r_{eff}	r_e(CP-opt)	r_{av}(CPMD)	exptl
$[Fe(CO)_5]$[a]	Fe–C(CO)	1.812	1.818	1.816	1.824	1.807/1.827[60]
$[Fe(CO)_3C_4H_4]$	Fe–C(CO)	1.786	1.792	1.780	1.790	1.80(3)[61]
	Fe–(C_4H_4)	2.063	2.072	2.071	2.087	2.06(2)[61]
$[Fe(CO)_3C_4H_6]$[b]	Fe–C(CO)	1.788	1.794	1.786	1.791	1.771/1.782(.9)[61]
	Fe–C^1	2.128	2.139	2.144	2.174	2.127(.3)[61]
	Fe–C^2	2.079	2.088	2.089	2.111	2.087(.2)[61]
$[Fe(CO)_4C_2H_3OMe]$[b]	Fe–C(CO)	1.804	1.810	1.802	1.811	
	Fe–C^1	2.207	2.223	2.248	2.301	
	Fe–C^2	2.137	2.149	2.162	2.192	
$[Fe(CO)_4C_2H_3CN]$[b]	Fe–C(CO)	1.812	1.817	1.813	1.822	
	Fe–C^1	2.108	2.119	2.116	2.140	
	Fe–C^2	2.135	2.146	2.142	2.176	
$[FeCp(CO)_2CH_3]$	Fe–C(CO)	1.752	1.757	1.738	1.743	
	Fe–C(CH_3)	2.062	2.072	2.056	2.077	
	Fe–C(Cp)	2.131	2.141	2.158	2.190	
$[FeCp(CO)_2C_3H_7]$	Fe–C(CO)	1.750	1.755	1.737	1.742	
	Fe–(C_3H_7)	2.116	2.129	2.112	2.159	
	Fe–C(Cp)	2.138	2.147	2.169	2.190	
$[Fe(CO)_3C_3H_4O]$	Fe–C(CO)	1.795	1.800	1.790	1.798	
	Fe–C(C_3H_4O)	2.088	2.097	2.098	2.117	
	Fe–O(C_3H_4O)	2.059	2.066	2.055	2.102	
$[FeCp_2]$	Fe–C(Cp)	2.054	2.062	2.055	2.068	2.058 ± 0.005[62]

[a] From ref. [26]. [b] See Figure 2 for numbering.

simulation time of 1.5 ps. The bond lengths of the model compound agree to ≈1 pm with $[VO(CH_2SiMe_3)_3]$.

In a few other cases, spontaneous conformational rearrangements were observed in the CPMD simulations. Specifically, methyl group rotations occurred in $[TiCl_2Me_2]$, $[TiClMe_3]$, $[TiMe_4]$, $[VOMe_3]$, $[VOMe_3AlH_3]$, and $[Fe(CO)_4C_2H_3OMe]$, and free Cp rotation was found in $[Mn(Cp)(C_7H_8)]$. Apparently, the corresponding barriers are so low that these rotations can be excited immediately after starting the simulations from the equilibrium geometry. For a peroxovanadate complex it was shown that the additional dynamical effect of such a ligand rotation on averaged geometrical parameters and chemical shifts is rather small.[71] Thus, no special care was taken in the present study to assess such rotational effects separately.

Chemical shifts: The chemical shifts of the metal centres computed at the equilibrium and the effective geometries, as well as the zero-point corrected and thermally averaged chemical shifts are listed in Tables 6–9. Both zero-point correction and thermal averaging result in a downfield shift of the magnetic shielding constant—the metal centre is deshielded.

The ^{49}Ti chemical shifts of the titanium complexes depend only marginally on the method of calculation. As already communicated previously for a somewhat larger test set of titanium compounds[28] the decrease of the shielding on going from δ_e to δ_0 is remarkably small, whereby the effect is solely due to the vibrational averaging of the geometry. We have assessed the effect due to thermal averaging by means of CPMD simulations, which find it a bit more pronounced than that of zero-point correction (compare σ_0 and σ_{av} values in Table 6). Compared with the static equilibrium values, the CPMD-derived thermal averages offer a minor improvement in terms of the mean absolute deviation, which decreases slightly from 130 ppm (CP-opt) to 110 ppm (CPMD).

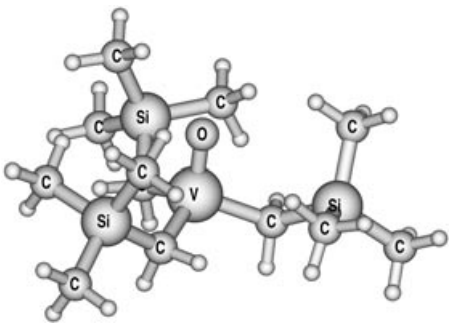

Figure 3. BP86/AE1 optimized geometry of $[VO(CH_2SiMe_3)_3]$.

Table 6. Equilibrium, effective, zero-point corrected and averaged chemical shifts [ppm] of the titanium complexes.

	δ_e(G98)[a]	δ_{eff}[a]	δ_0[a]	δ_e(CP-opt)	δ_{av}(CPMD)	exptl
$[Ti(CO)_6]^{2-}$	−1646	−1647	−1644	−1650	−1616	−1389[2]
$[TiCp_2F_2]$	−1245	−1237	−1234	−1230	−1163	−1037[84]
$[TiCp_2Cl_2]$	−892	−878	−874	−915	−838	−772[84]
$[TiCl_3Me]$	443	445	444	465	478	613[85]
$[TiCl_2Me_2]$	796	801	799	788	788	907[85]
$[TiClMe_3]$	1077	1036	1034	1096	1044	1188[85]
$[TiMe_4]$	1317	1314	1312	1290	1253	1325[2]
slope[b]	1.05	1.05	1.05	1.06	1.02	
axis intercept[b]	−147	−149	−148	−148	−129	
mean abs. dev.[c]	141	126	126	130	110	

[a] From ref. [28]. [b] From a linear regression analysis with respect to the experimental value. [c] Mean absolute deviation from experiment.

Table 7. Equilibrium, effective, zero-point corrected and averaged chemical shifts [ppm] of the vanadium complexes.

	δ_e(G98)	δ_{eff}	δ_0	δ_e(CP-opt)	δ_{av}(CPMD)	exptl
$[V(CO)_6]^-$	−2279	−2274	−2269	−2305	−2196	−1952[2]
$[V(CO)_5N_2]^-$	−2028	−2017	−2011	−2075	−1982	−1671[2]
$[VF_5]$	−913	−913	−913	−972	−946	−895[2]
$[VOF_3]$	−887	−889	−889	−897	−908	−757[2]
$[VOClF_2]$	−602	−604	−603	−618	−616	−582[2]
$[VO(OCH_2CH_2)_3N]$	−459	−461	−459	−457	−466	−380[2]
$[VOCl_2F]$	−302	−303	−303	−323	−308	−341[2]
$[VO(CH_3)_3]$	1072	1087	1082	1042	1043	1205[86],[a]
$[VO(CH_3)_3AlH_3]$	1418	1429	1426	1359	1444	1575[86],[a]
slope[b]	1.04	1.05	1.04	1.04	1.03	
axis intercept[b]	−113	−108	−109	−144	−114	
mean abs. dev.[c]	140	136	135	165	134	

[a] -CH_2SiMe_3 derivatives. [b] From a linear regression analysis with respect to the experimental value. [c] Mean absolute deviation from experiment.

Table 8. Equilibrium, effective, zero-point corrected and averaged chemical shifts [ppm] of the manganese complexes.

	δ_e(G98)	δ_{eff}	δ_0	δ_e(CP-opt)	δ_{av}(CPMD)	exptl
$[Mn(CO)_5]^-$	−2819	−2828	−2817	−2846	−2651	−2780[87]
$[Mn(CO)_5H]$	−2974	−2962	−2949	−2967	−2783	−2578[2]
$[MnCp(CO)_3]$	−2331	−2290	−2280	−2297	−2002	−2225[2]
$[Mn(CO)_5(COMe)]$	−2230	−2203	−2192	−2223	−1940	−1851[2]
$[Mn(NO)_3(CO)]$	−1160	−1149	−1137	−1140	−912	−1171[2]
$[Mn(CO)_5Cl]$	−1749	−1706	−1694	−1773	−1434	−1004[2]
$[MnCp(C_7H_8)]$	734	863	885	776	1410	1077[2]
slope[a]	0.96	0.98	0.98	0.96	1.06	
axis intercept[a]	−339	−286	−269	−344	+126	
mean abs. dev.[b]	288	255	246	286	238	

[a] From a linear regression analysis with respect to the experimental value. [b] Mean absolute deviation from experiment.

The ^{51}V chemical shifts of the vanadium complexes are all too low (i.e., shifted upfield) with regard to the experiment. Thermal averaging or zero-point correction both lead to a deshielding of the vanadium nuclei and, thus, to a decrease in the average deviation from the experimental values (see Table 7; Figures 4 and 5). But as the bond lengths r_{eff} and r_{av} are not very different from the optimized geometries r_e, the effect on the magnetic shielding constants is not very large either. The average deviation only decreases from 165 ppm (CP-opt) to 134 ppm (CPMD) (Table 7). We have computed the ^{51}V chemical shift of both $[VO(CH_2SiMe_3)_3]$ and its model compound $[VOMe_3]$. The chemical shifts at the equilibrium geometry agree to 5 ppm (G98) and 19 ppm (CP-opt) respectively, which is significantly lower than the absolute error of the calculated chemical shifts. Thus, the use of the model compound is well justified.

The ^{55}Mn chemical shifts of the manganese complexes, referenced directly to $[MnO_4]^-$, show the largest average deviation from the experimental chemical shifts. Similar to the titanium and vanadium complexes, the chemical shifts at the optimized geometries are all shifted upfield with respect to the experimental values. As noted before, this deviation in $\delta(^{55}Mn)$ is systematic (roughly 300 ppm) and can be reduced by choosing a different σ value for the standard, for example, one derived from a correlation of computed σ versus experimental δ values.[29] It had initially been speculated that this systematic deviation with respect to free $[MnO_4]^-$ could be due to the neglect of sovation effect on the latter (experiments are conducted in water for the standard, and in more inert solvents for the organomanganese species). However, this possibility was subsequently refuted in a CPMD study of $\sigma(^{55}Mn)$ of aqueous $[MnO_4]^-$.[16] Since the computed thermal effects were very small for this inorganic complex, part of the systematic deviations might be explained by much larger thermal effects for the organomanganese substrates. For $\sigma(^{57}Fe)$ in $Fe(CO)_5$, for example, deshieldings on the order of 250–300 ppm have been obtained by CPMD and BOMD simulations.[15,72] A similarly large decrease of the CPMD-averaged $\sigma(^{55}Mn)$ values is obtained for the organomanganese species, which, together with the small thermal deshielding of the standard (−35 ppm[16]), leads to downfield shifts of the $\delta(^{55}Mn)$ data by about ≈200–300 ppm in most cases (compare CP-opt and CPMD entries in Table 8). An exceptionally large effect is found for $[MnCp(C_7H_8)]$, with $\delta_{av}-\delta_e$ exceeding 600 ppm. For this compound, the error in δ_e is overcorrected to such an extent that the slope of the $\delta_{calcd}/\delta_{exptl}$ correction deteriorates from the near-ideal value close to 1 to 1.06. Most of

Table 9. Equilibrium, effective, zero-point corrected and averaged chemical shifts [ppm] of the iron complexes.

	δ_e(G98)	δ_{eff}	δ_0	δ_e(CP-opt)	δ_{av}(CPMD)	exptl
$[Fe(CO)_3C_4H_4]$	−514	−490	−490	−561	−513	−583[2]
$[Fe(CO)_3C_4H_6]$	25	70	72	76	171	4[2]
$[Fe(CO)_4C_2H_3OCH_3]$	151	187	191	173	310	5[88]
$[Fe(CO)_4C_2H_3CN]$	202	223	225	205	311	303[88]
$[FeCp(CO)_2CH_3]$	786	865	872	871	1110	684[89]
$[FeCpC_3H_7]$	960	1043	1051	1102	1391	796[89]
$[Fe(CO)_2C_3H_4O]$	1223	1296	1299	1194	1429	1274[2]
$[FeCp_2]$	1465	1557	1561	1524	1773	1532[2]
slope[a]	0.95	0.98	0.98	0.98	1.09	
axis intercept[a]	61	101	103	81	202	
mean abs. dev.[b]	90	112	115	118	246	

[a] From a linear regression analysis with respect to the experimental value. [b] Mean absolute deviation from experiment.

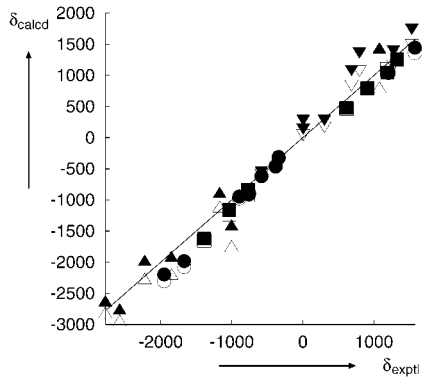

Figure 4. Plot of computed (GIAO-B3LYP for CP-opt and thermally averaged geometries, CPMD) versus experimental chemical shifts. □: Ti(CP-opt), ○: V(CP-opt), △: Mn(CP-opt), ▽: Fe(CP-opt), ■: Ti(CPMD), ●: V(CPMD), ▲: Mn(CPMD), ▼: Fe(CPMD).

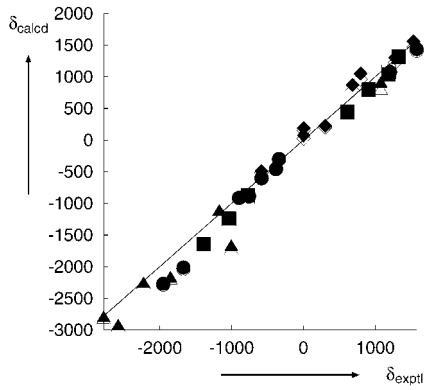

Figure 5. Plot of computed (GIAO-B3LYP for BP86/AE1 optimized and zero-point corrected geometries, ZPC) versus experimental chemical shifts. □: Ti(opt), ○: V(opt), △: Mn(opt), ▽: Fe(opt), ■: Ti(ZPC), ●: V(ZPC), ▲: Mn(ZPC), ▼: Fe(ZPC).

the other δ_{av} data are improved over the δ_e values, however, so that the overall mean absolute deviation is reduced from 286 to 238 ppm. The zero-point correction also produces downfield shifts of $\delta(^{55}Mn)$, but this is much too small to correct the mean absolute error (compare δ_e and δ_0 values in Table 8), and the deviation only decreases from 288 to 246 ppm. Thus, both CPMD based and perturbational methods afford only marginal improvements of the overall manganese chemical shifts.

The equilibrium ^{57}Fe chemical shifts of the iron complexes agree quite well with the experimental data. The mean absolute deviation of $\delta_e(^{57}Fe)$ falls between 90 and 118 ppm (see Table 9). Approximately half of the iron complexes tested exhibit a downfield shift with regard to the experimental value, while the other half exhibit an upfield shift. The downfield shift due to the thermal averaging or the zero-point correction overestimates the deshielding of the metal centres. This effect is especially pronounced in the CPMD results for the cyclopentadienyl- and acrolein complexes at the deshielded end, so that the average deviation increases from 118 to 246 ppm (compare CP-opt and CPMD data in Table 9). As with the nuclei discussed above, the computed zero-point corrections to $\delta(^{57}Fe)$ are much smaller than the CPMD-derived thermal effects, but follow the same trend. Thus, the δ_0 values are not improved over their δ_e counterparts, and the mean deviation increases slightly from 90 to 110 ppm (Table 9). At least in the test set of this study, no qualitative changes in the overall pattern of δ values is introduced upon inclusion of vibrational or thermal corrections. For instance, at all levels very similar resonances (within 50 ppm at most) are computed for the two olefin complexes $[Fe(CO)_4C_2H_3X]$, X = OMe and CN, despite the fact that the experimental shifts differ by nearly 300 ppm. This apparent inconsistency is thus not resolved upon inclusion of thermal corrections, and appears to be inherent to the DFT levels applied.

Another probe for the quality of theoretical results is the slope of the regression line from the correlation of calculated versus experimental chemical shifts, which, in the ideal case would assume the value 1.00. In general the slopes of the regression lines are not affected much by the zero-point correction—the maximum difference between δ_e and δ_0 data in Tables 6–9 is 0.03 in case of the iron complexes. The effect of the thermal averaging on the slopes of the regression lines is more pronounced: on going from the CP-opt to the CPMD data the results can be slightly improved (Ti and V complexes) or worsened (Mn and Fe complexes).

The slopes of the regression lines of the δ_{eff} and δ_0 data are very similar. The computed values for the individual molecules show that the difference $\delta_0 - \delta_{eff}$ in general amounts up to a few ppm only. The main effect of the zero-point correction is thus due to the vibrational averaging of the geometry; the effect due to the expansion of the magnetic shielding constant at the effective geometry seems to be less pronounced. For further calculations of vibrational corrections to transition metal chemical shifts it is therefore sufficient to limit the calculation to the determination of σ_{eff}. This allows for significant savings in CPU time, as the additional $6N-11$ property evaluations (N = number of atoms)

required for determining σ_0 are not necessary. In summary, classical thermal averaging assessed via CPMD simulations, and zero-point corrections evaluated perturbationally, afford the same qualitative effects on transition metal chemical shifts. In general, the metal nuclei are deshielded, typically by an increasing magnitude with a higher δ value. The sensitivity of the metals towards the thermal and vibrational corrections increases from Ti to Fe. Computed zero-point effects on the metal shifts are significantly smaller than the classical thermal effects estimated from CPMD simulations.

Discussion

It should be recalled at this point that by contrasting classical thermal averages and zero-point effects, two very different things are compared. Thus, it is for example not possible to regard both as independent increments and simply add them up. Classical MD-derived thermal effects would best be compared with quantum thermal effects at the same temperature. Such effects can be evaluated, for instance, by explicit summation over rovibrationally averaged shieldings weighted by Boltzmann factor[17] or by suitable quantum Monte Carlo approaches.[18] For light main-group molecules the corresponding quantum thermal effects, that is, the difference between the zero-point values and those at room temperature, have been shown to be much smaller than the zero-point corrections themselves. It would be very interesting to see if the same holds true for the transition-metal complexes of this study. Unfortunately, these rigorous methods are intractable or impractical for molecules this large. In principle, the more approximate perturbational approach that we have employed for the zero-point corrections can be extended to evaluate effective geometries and averaged properties at thermal equilibrium for a given temperature.[73,74] To our knowledge, however, systematic tests and benchmarks for this method have not yet reported.[75] Clearly, further research efforts in this direction are warranted.

Despite this incompatibility of classical MD-based averages and quantum mechanical zero-point corrections in terms of the underlying theoretical model, the effects obtained with either method have the same physical origin, namely the anharmonicity of the PES and the curvature of the magnetic shielding hypersurface in the vicinity of the equilibrium geometry. It is thus sensible to discuss the results for both methods together, in particular with respect to the interdependence of averaged geometries and chemical shifts, which is analyzed in more detail in the following.

Of the geometrical parameters that affect the chemical shift of a metal, the bond lengths to its ligands are usually the most important ones,[76,77] even in cases where bond angles had been initially believed to be decisive.[76] The sensitivity towards these parameters can be quantified in terms of the shielding/bond-length derivatives, $\partial\sigma_M/\partial r_{M-L}$. Sizeable values of this quantity have been estimated from experiment, for example, $\partial\sigma_{Co}/\partial r_{Co-L} = -80\ \mathrm{ppm\,pm^{-1}}$ in $[Co(CN)_6]^{3-}$[78] (a value which has been well reproduced at the B3LYP level),[79] and even larger ones have been predicted computationally, for example, $\partial\sigma_{Fe}/\partial r_{Fe-L} = -320\ \mathrm{ppm\,pm^{-1}}$ in $[Fe(CN)_6]^{4-}$.[72] We have evaluated salient shielding/bond-length derivatives for the test molecules of the present study, employing the following procedure: The magnetic shielding constants σ have been computed at the B3LYP/II′ level for geometries, in which the bond lengths to each of symmetry-equivalent ligand atoms have been distorted from their equilibrium values (a total of five displaced geometries have been generated; with Δr ranging from -1 to $+3$ pm) leaving all other parameters unchanged, and the $\partial\sigma_M/\partial r_{M-L}$ derivatives have been determined by linear regression (see Tables 10–13).

Table 10. Shielding/bond-length derivative $\partial\sigma_{Ti}/\partial r_{Ti-L}$ in titanium compounds; see text for details.

		$\partial\sigma_{Ti}/\partial r_{Ti-L}$ [ppm pm^{-1}]	"per bond"[a]
$[Ti(CO)_6]^{2-}$	$Ti-(CO)_6$	−18.4	−3.1
$[TiCp_2F_2]$	Ti−Cp	−3.7	−3.7
	$Ti-F_2$	−13.6	−6.8
$[TiCp_2Cl_2]$	Ti−Cp	−7.0	−7.0
	$Ti-Cl_2$	−11.8	−5.9
$[TiCl_4]$	$Ti-Cl_4$	−27.7	−6.9
$[TiCl_3Me]$	Ti−Me	−10.4	−10.4
	$Ti-Cl_3$	−23.2	−7.7
$[TiCl_2Me_2]$	$Ti-Me_2$	−20.5	−10.3
	$Ti-Cl_2$	−20.5	−10.3
$[TiClMe_3]$	$Ti-Me_3$	−28.2	−9.4
	Ti−Cl	−7.7	−7.7
$[TiMe_4]$	$Ti-Me_4$	−33.9	−8.5

[a] π Ligands counted as single ligand.

Table 11. Shielding/bond-length derivative $\partial\sigma_V/\partial r_{V-L}$ in vanadium compounds; see text for details.

		$\partial\sigma_V/\partial r_{V-L}$ [ppm pm^{-1}]	"per bond"
$[V(CO)_6]^-$	$V-(CO)_6$	−44.5	−7.4
$[V(CO)_5N_2]^-$	V−N	−8.3	−8.3
	$V-(CO)_5$	−41.7	−8.3
$[VF_5]$	$V-F_5$	−58.8	−11.8
$[VOF_3]$	V−O	−34.0	−34.0
	$V-F_3$	−33.3	−11.1
$[VClF_2]$	V−O	−35.6	−35.6
	V−Cl	−8.3	−8.3
	$V-F_2$	−20.6	−10.3
$[VO(OCH_2CH_2)_3N]$	V−O	−32.7	−32.7
	$V-O_3$	−41.3	−13.8
	V−N	−2.9	−2.9
$[VOCl_2F]$	V−O	−37.2	−37.2
	V−F	−13.2	−13.2
	$V-Cl_2$	−20.5	−10.3
$[VOCl_3]$	V−O	−32.2	−32.2
	$V-Cl_3$	−36.5	−14.2
$[VO(CH_3)_3]$	V−O	−43.3	−43.3
	$V-(CH_3)_3$	−71.7	−23.9
$[VO(CH_2Si(CH_3)_3)_3]$	V−O	−42.5	−42.5
	V−$(CH_2Si(CH_3)_3)_3$	−72.1	−24.0
$[VO(CH_3)_3AlH_3]$	V−O	−39.7	−39.7
	$V-(CH_3)_3$	−88.3	−29.4

When looking at the results normalized to the number of equivalent ligands ("per bond" entries in Tables 6–9) it becomes apparent that the sensitivity of the metal nucleus to the distances to its ligands increases in the sequence Ti <

Table 12. Shielding/bond-length derivative $\partial\sigma_{Mn}/\partial r_{Mn-L}$ in manganese compounds; see text for details.

		$\partial\sigma_{Mn}/\partial r_{Mn-L}$ [ppm pm^{-1}]	"per bond"[a]
$[Mn(CO)_5]^-$	Mn−$(CO)_5$	−126.5	−25.3
$[Mn(CO)_5H]$	Mn−H	−13.8	−13.8
	Mn−$(CO)_5$	−119.5	−23.9
$[MnCp(CO)_3]$	Mn−Cp	−65.4	−65.4
	Mn−$(CO)_3$	−120.1	−40.0
$[Mn(CO)_5(COMe)]$	Mn−C(COMe)	−6.0	−6.0
	Mn−$(CO)_5$	−134.6	−26.9
$[Mn(NO)_3(CO)]$	Mn−$(NO)_3$	−144.3	−48.1
	Mn−CO	−38.4	−38.4
$[Mn(CO)_5Cl]$	Mn−Cl	−10.3	−10.3
	Mn−$(CO)_5$	−171.2	−34.2
$[MnO_4]^-$	Mn−O_4	−170.0	−42.5[b]
$[MnCp(C_7H_8)]$	Mn−Cp	−155.5	−155.5
	Mn−C_7H_8	−112.4	−112.4

[a] π Ligands counted as single ligand. [b] From ref. [16].

Table 13. Shielding/bond-length derivative $\partial\sigma_{Fe}/\partial r_{Fe-L}$ in iron compounds; see text for details.

		$\partial\sigma_{Fe}/\partial r_{Fe-L}$ [ppm pm^{-1}]	"per bond"[a]
$[Fe(CO)_3C_4H_4]$	Fe−C_4H_4	−55.4	−55.4
	Fe−$(CO)_3$	−87.4	−29.1
$[Fe(CO)_5]$	Fe−$(CO)_5$	−170.4	−34.1
$[Fe(CO)_3C_4H_6]$	Fe−C_4H_6	−55.6	−55.6
	Fe−$(CO)_3$	−106.4	−35.5
$[Fe(CO)_4C_2H_3CN]$	Fe−C_2H_3CN	−23.9	−23.9
	Fe−$(CO)_4$	−159.8	−40.0
$[Fe(CO)_4C_2H_3OCH_3]$	Fe−$C_2H_3OCH_3$	−20.8	−20.8
	Fe−$(CO)_4$	−155.3	−38.8
$[FeCp(CO)_2CH_3]$	Fe−CH_3	−18.7	−18.7
	Fe−Cp	−92.4	−92.4
	Fe−$(CO)_2$	−113.9	−57.0
$[FeCp(CO)_2C_3H_7]$	Fe−C_3H_7	−18.7	−18.7
	Fe−Cp	−90.0	−90.0
	Fe−$(CO)_2$	−117.6	−58.8
$[Fe(CO)_3C_3H_4O]$	Fe−C_3H_4O	−63.9	−63.9
	Fe−$(CO)_3$	−143.9	−48.0
$[FeCp_2]$	Fe−Cp_2	−232.1	−116.1

[a] π Ligands counted as single ligand.

V < Mn < Fe. For instance, the $\partial\sigma_M/\partial r_{M-CO}$ value in the homoleptic carbonyl compounds grows monotonically from $[Ti(CO)_6]^{2-}$ (−3 ppm pm^{-1}) via $[V(CO)_6]^-$ (−7 ppm pm^{-1}) and $[Mn(CO)_5]^-$ (−25 ppm pm^{-1}) to $[Fe(CO)_5]$ (−34 ppm pm^{-1}). To explain the reason of this monotonical increase, one has to consider the effects that can influence the chemical shift. Usually the magnetic shielding is partioned into a diamagnetic and a paramagnetic part in Equation (3):

$$\sigma = \sigma^d + \sigma^p \quad (3)$$

It has been observed that the diamagnetic part is only marginally influenced by the chemical environment and therefore, does not contribute noticeably to the relative chemical shift.[80] The leading contribution to the paramagnetic shielding is pictured physically as an induced paramagnetic current in the system and originates from a coupling between the occupied (ϕ_i with orbital energy ε_i) and virtual (ϕ_a with orbital energy ε_a) MOs. The magnitude of this term is proportional to[80,81] Equation (4):

$$-\frac{1}{\varepsilon_i^{(0)} - \varepsilon_a^{(0)}} \langle \phi_i | \hat{M} | \phi_a \rangle \quad (4)$$

The magnetic operator $\hat{M}$ affects the ϕ_a such that it rotates the orbital around its position, that is, the *y* component of the operator rotates the p_z orbital into an orbital proportional to the p_x orbital.[82] Schreckenbach showed that the paramagnetic shielding of $[Fe(CO)_5]$ is dominated by transitions between frontier orbitals with d character, so that the chemical shift is governed by the energy difference of the occupied and virtual d-type orbitals.[80] The detailed list of the contributions to the paramagnetic shielding revealed that a number of occupied→virtual transitions provide contributions of similar magnitude (i.e., Schreckenbach mentioned seven significant contributions to the paramagnetic shielding of $[Fe(CO)_5]$).[80] To estimate the occupied→virtual contributions to the paramagnetic shielding for the four carbonyl compounds we took the HOMO–LUMO gap as a measure and calculated the HOMO–LUMO gap at the five different structures used for the calculation of the shielding/bond-length derivative. The linear regression of the energy differences (regression coefficient = 1.00) yields slopes of −1.33, −1.75, −2.03, and -2.16×10^{-3} a.u. pm^{-1}, for $[Ti(CO)_6]^{2-}$, $[V(CO)_6]^-$, $[Mn(CO)_5]^-$, and $[Fe(CO)_5]$, respectively. Thus, the increasing shielding/bond-length derivative on going from Ti to Fe complexes is consistent with the increasing sensitivity of the HOMO–LUMO gap of the M−CO bond length and therefore, ultimately to the increasing metal−carbonyl bond strength.

The matrix element in the numerator of Equation (4) depends on the overlap of the "rotated" orbital, $\hat{M}|\phi_a\rangle$, with the unperturbed $\langle\phi_i|$. For the metal shielding, these contributions increase with the magnitude of the d orbital character in the respective orbitals. To estimate this part of the term we chose the HOMO of each carbonyl complex as a representative example and calculated its d-orbital character by summing up the squares of the respective d-orbital contributions. In principle we have to investigate the d-orbital character of all possibly involved frontier orbitals. However, from our calculations it is not possible to deduce which of the d→d transitions is the dominating one. Therefore we limit our investigation of the estimation of the d character of the HOMO as a representative example, which is sufficient for our purpose to describe the sensitivity of the magnetic shielding qualitatively. The magnitude of the d-orbital character in the HOMO follows the relative order 1:1.17:1.47:1.57 for $[Ti(CO)_6]^{2-}$, $[V(CO)_6]^-$, $[Mn(CO)_5]^-$ and $[Fe(CO)_5]$, respectively. Thus, both energies and shape of the frontier molecular orbitals strengthen the sensitivity of the magnetic shielding to the M−CO bond length on going from Ti to Fe complexes.

The shielding/bond-length derivatives involving a particular ligand are not transferable between complexes of a given metal. The more deshielded the metal resonance is, the more sensitve it appears towards the bond length. For example, the $\partial\sigma_{Fe}/\partial r_{Fe-CO}$ values in iron carbonyl complexes are, ordered according to decreased shielding of the iron centre, −29, −34, −40, −39, −57, −59, and −48 ppm pm^{-1} in $[Fe(CO)_3(C_4H_4)]$, $[Fe(CO)_5]$, $[Fe(CO)_4(C_2H_3CN)]$, $[Fe(CO)_4(C_2H_3OMe)]$, $[FeCp(CO)_2Me]$, $[FeCp(CO)_2C_3H_7]$, and $[Fe(CO)_3(C_3H_4O)]$, respectively. For the iron and the manganese complexes, the six-electron π ligands exert the strongest effect on the magnetic shielding of the metal centre, in particular the Mn–Cp and the Fe–Cp distances up to −156 and −116 ppm pm^{-1}, respectively. The magnetic shieldings of the vanadium and titanium complexes show a weaker dependence on the metal–ligand separations. The largest shielding/bond-length derivative involving these metals is attributed to the terminal V–O bond in the oxovanadium complexes with values of about −40 ppm pm^{-1} and to the Ti–CH_3 bond with about −10 ppm pm^{-1}.

To what extent can the differences between equilibrium magnetic shielding constants and their thermal averages be traced back to the elongation of the metal–ligand bonds? For an estimate of the latter effect, we have multiplied the elongation of each metal–ligand bond with the appropriate shielding/bond-length derivative and summed up all the products for each molecule.

In Table 14 this estimated difference $(\sigma_e-\sigma_{av})_{estd}$ is compared with the actual difference in the magnetic shielding, as calculated on the basis of the MD simulations (σ_e(CP-opt) $-\sigma_{av}$(CPMD) entry in Table 14, for a graphical representation see Figure 6). For the vanadium and some of the titanium complexes, the actual difference in the magnetic shielding is indeed approximately as big as the estimated one. For manganese and iron complexes, in contrast, the actual differences (σ_e(CP-opt)−σ_{av}(CPMD)) are significantly larger than those estimated from the shielding/bond-length derivatives. Thus, the elongation of the metal–ligand bonds accounts for a large part of the downfield shift due to the thermal averaging (ca. 63%, judging from the slope of the regression line in Figure 6), but apparently is not the only reason. It is possible that the downfield shift due to the elongation of individual bonds is not an additive effect, as assumed in our analysis, or that changes in the bond angles or internal rotations as mentioned in the geometries section may also play a significant role for vibrational and thermal corrections to the magnetic shieldings. Earlier attempts to derive increment systems for transition metal chemical shifts (for ^{109}Rh, specifically) have also met with limited success.[76]

A similar analysis is included in Table 14 for the $(\sigma_e-\sigma_{eff})$ values (see Figure 7 for a plot). Since the bond elongation between r_e and r_{eff} is much smaller than that between r_e and r_{av}; the resulting $(\sigma_e-\sigma_{eff})$ data span a smaller range than the $(\sigma_e-\sigma_{av})$ values. A common trend between $(\sigma_e-\sigma_{eff})_{estd}$ and $(\sigma_e-\sigma_{eff})_{calcd}$ is clearly visible (Figure 7). Interestingly, the slope of the regression line involving $(\sigma_e-\sigma_{eff})$, 1.02, is much closer to unity than that for the $(\sigma_e-\sigma_{av})$ data. Possibly, for the smaller elongations as occurring in the CPMD simulations for Ti and V complexes, or in the zero-point vibrationally averaged structures of all species of this study, the above-mentioned effects of non-additivity are less pronounced, and our simple analysis can afford a reasonable

Table 14. Difference between thermally averaged and equilibrium magnetic shieldings $\sigma_e-\sigma_{av}$.[a]

	$(\sigma_e-\sigma_{eff})_{estd}$	$(\sigma_e-\sigma_{eff})_{calcd}$	$(\sigma_e-\sigma_{av})_{estd}$	$(\sigma_e-\sigma_{av})_{calcd}$
$[Ti(CO)_6]^{2-}$	13	6	−2	52
$[TiCp_2F_2]$	7	14	13	84
$[TiCp_2Cl_2]$	10	21	31	94
$[TiCl_4]$	8	7	17	17
$[TiCl_3Me]$	7	7	31	30
$[TiCl_2Me_2]$	8	11	41	17
$[TiClMe_3]$	7	35	18	35
$[TiMe_4]$	3	3	14	19
$[V(CO)_6]^-$	27	22	31	137
$[V(CO)_5N_2]^-$	33	28	59	120
$[VF_5]$	18	17	41	41
$[VOF_3]$	17	15	20	17
$[VOClF_2]$	14	15	22	30
$[VO(OCH_2CH_2)_3N]$	20	15	18	19
$[VOCl_2F]$	15	16	30	43
$[VOCl_3]$	14	17	15	28
$[VOMe_3]$	16	21	63	29
$[VOMe_3AlH_3]$	38	38	175	113
$[Mn(CO)_5]^-$	51	51	114	230
$[Mn(CO)_5H]$	81	72	112	219
$[MnCp(CO)_3]$	118	101	207	330
$[Mn(CO)_5(COMe)]$	86	87	152	318
$[Mn(NO)_3(CO)]$	66	71	112	263
$[Mn(CO)_5Cl]$	124	103	220	374
$[MnO_4]^-$	51	60	34	35
$[MnCp(C_7H_8)]$	214	189	511	669
$[Fe(CO)_3C_4H_4]$	102	106	176	317
$[Fe(CO)_5]$	102	82	136	269
$[Fe(CO)_3C_4H_6]$	114	127	198	364
$[Fe(CO)_4C_2H_3OCH_3]$	122	118	227	406
$[Fe(CO)_4C_2H_3CN]$	106	103	213	375
$[FeCp(CO)_2CH_3]$	168	161	392	508
$[FeCpC_3H_7]$	164	165	336	558
$[Fe(CO)_2C_3H_4O]$	123	155	326	504
$[FeCp_2]$	168	174	302	537

[a] estd: estimated using the shilding/bond-length derivatives from Tables 10–13 multiplied with the corresponding differences in bond lengths from Tables 2–5; calcd: actual calculated differences from Tables 6–9. The corresponding data (estimated and calculated) are given for the equilibrium and effective geometries.

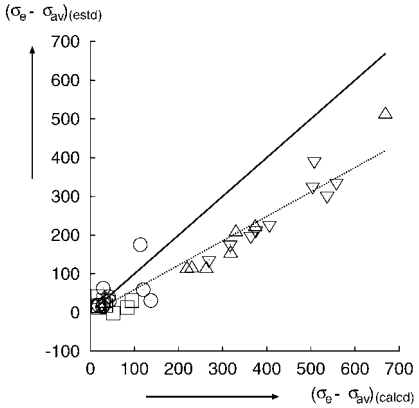

Figure 6. Plot of the estimated vs calculated difference between thermally averaged and equilibrium magnetic shieldings $\sigma_e-\sigma_{av}$; data from Table 14; ——: ideal slope, •••••: linear regression; □: Ti, ○: V, △: Mn, ▽: Fe.

description and interpretation of the thermal effects on the metal shifts.

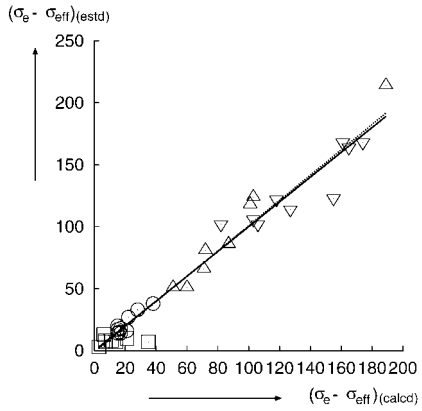

Figure 7. Plot of the estimated versus calculated difference between effective and equilibrium magnetic shieldings $\sigma_e - \sigma_{eff}$; data from Table 14; ——: ideal slope, •••••: linear regression; □: Ti, ○: V, △: Mn, ▽: Fe.

Conclusion

We have assessed different methods for computation of the chemical shift of metal centres in selected examples of Ti, V, Mn and Fe complexes, methods that go beyond simple calculations of equilibrium values for static optimized structures. Classical thermal effects on the chemical shifts have been modelled by performing CPMD simulations, and quantum mechanical zero-point corrections have been evaluated using a perturbational approach. Both methods lead to a decrease of the absolute magnetic shielding constants σ from their equilibrium values (i.e., the metal centre is deshielded). This effect can to a large extent be explained by the elongation of the metal-ligand bond lengths in the averaged or effective geometries, as compared to the equilibrium distances. In terms of relative chemical shifts δ, the application of these two methods leads to an improvement of the results in selected cases, but not in general. In most cases the equilibrium chemical shifts at the optimized geometry are shifted upfield with respect to the experimental values. The downfield shifts due to the thermal averaging, or the zero-point correction can be too small (Ti and V complexes) or too large (some Mn and Fe complexes). The overcorrection in the latter cases is particularly pronounced for the CPMD-based classical thermal averaging. In summary, inclusion of thermal or vibrational corrections does not lead to a systematic improvement of theoretical transition-metal shifts. Such corrections can be noticeable, but are usually much smaller than differences between results obtained with different exchange-correlation functionals (in particular "pure" gradient-corrected vs hybrid variants). Thus, the most promising route to improved chemical shifts for this class of compounds appears to be that via development of better density functionals, and/or via inclusion of solvent effects, which we will explore in future investigations.

[1] *Encyclopedia of Nuclear Magnetic Resonance* (Eds.: D. M. Grant, R. K. Harris), Wiley, New York, **1996**.
[2] *Transition Metal Nuclear Magnetic Resonance* (Ed.: P. S. Pregosin), Elsevier, Amsterdam, **1991**.
[3] S. Gaemers, C. J. Elsevier, *Chem. Soc. Rev.* **1999**, *28*, 135.
[4] W. von Philipsborn, *Chem. Soc. Rev.* **1999**, *28*, 95.
[5] W. Koch, M. C. Holthausen *A Chemist's Guide to Density Functional Theory*, Wiley-VCH, Weinheim, **2000**.
[6] M. Kaupp in *Encyclopedia of Computational Chemistry*, *Vol. 3* (Eds.: P. v. R. Schleyer, N. L. Allinger, P. A. Kollman, T. Clark, H. F. Schaefer, J. Gasteiger, P. R. Schreiner), Wiley, Chichester, **1998**, pp. 1857.
[7] G. Schreckenbach, T. Ziegler, *Theor. Chem. Acc.* **1998**, *99*, 71.
[8] M. Bühl, M. Kaupp, M. Malkin, V. G. Malkina, *J. Comput. Chem.* **1999**, *20*, 91.
[9] M. Bühl in *Calculation of NMR and EPR Parameters. Theory and Applications* (Eds.: M. Kaupp, M. Bühl, V. G. Malkin), Wiley-VCH, Weinheim, **2004**, pp. 421.
[10] M. Bühl, *Chem. Phys. Lett.* **1997**, *267*, 251.
[11] M. Bühl, F. A. Hamprecht, *J. Comput. Chem.* **1998**, *19*, 113.
[12] R. Car, P. Parrinello, *Phys. Rev. Lett.* **1985**, *55*, 2471.
[13] V. G. Malkin, O. L. Malkina, G. Steinebrunner, H. Huber, *Chem. Eur. J.* **1996**, *2*, 452.
[14] M. Bühl, M. Parrinello, *Chem. Eur. J.* **2001**, *7*, 4487.
[15] M. Bühl, F. T. Mauschick, *Phys. Chem. Chem. Phys.* **2002**, *4*, 5508.
[16] M. Bühl, *J. Phys. Chem. A* **2002**, *106*, 10505.
[17] D. Sundholm, J. Gauss, A. Schäfer, *J. Chem. Phys.* **1996**, *105*, 11051.
[18] M. C. Böhm, J. Schulte, R. Ramírez, *Int. J. Quantum Chem.* **2002**, *86*, 28.
[19] A. A. Auer, J. Gauss, J. F. Stanton, *J. Chem. Phys.* **2003**, *118*, 10407.
[20] W. T. Raynes, M. Nightingale, *Int. J. Quantum Chem.* **1996**, *60*, 529.
[21] C. H. Gee, W. T. Raynes, *Chem. Phys. Lett.* **2000**, *330*, 595.
[22] K. Ruud, P.-O. Åstrand, P. R. Taylor, *J. Am. Chem. Soc.* **2001**, *123*, 4826.
[23] K. Ruud, P.-O. Åstrand, P. R. Taylor, *J. Chem. Phys.* **2000**, *112*, 2668.
[24] T. Ruden, O. B. Lutnæes, T. Helgaker, *J. Chem. Phys.* **2003**, *118*, 9572.
[25] P.-O. Åstrand, K. Ruud, *Phys. Chem. Chem. Phys.* **2003**, *5*, 5015.
[26] M. Bühl, P. Imhof, M. Repisky, *ChemPhysChem* **2004**, *5*, 410.
[27] These values mark essentially the actual, observed chemical shift ranges except for ^{57}Fe, where a few compounds with outstanding $\delta(^{57}\text{Fe})$ values, such as myoglobin derivates, increase the total chemical shift range to ca. 9000 ppm, see ref. [2].
[28] M. Bühl, F. T. Mauschick, *Magn. Reson. Chem.* **2004**, *42*, 737.
[29] M. Bühl, *Theor. Chem. Acc.* **2002**, *107*, 336.
[30] M. Bühl, O. L. Malkina, V. G. Malkin, *Helv. Chim. Acta* **1996**, *79*, 742.
[31] A. D. Becke, *Phys. Rev. A* **1988**, *38*, 3098.
[32] J. P. Perdew, *Phys. Rev. B* **1986**, *33*, 8822.
[33] J. P. Perdew, *Phys. Rev. B* **1986**, *34*, 7406.
[34] A. J. H. Wachters, *J. Chem. Phys.* **1970**, *52*, 1033.
[35] P. J. Hay, *J. Chem. Phys.* **1977**, *66*, 4377.
[36] G. L. Karapinka, J. J. Smith, W. L. Carrick, *J. Polym. Sci.* **1961**, *50*, 143.
[37] D. C. Crans, H. Chen, D. P. Anderson, M. M. Miller, *J. Am. Chem. Soc.* **1993**, *115*, 6769.
[38] W. F. Edgel, J. W. Fisher, G. Asato, W. M. Risen Jr., *Inorg. Chem.* **1969**, *8*, 1103.
[39] R. J. Sullivan, T. L. Brown, *J. Am. Chem. Soc.* **1991**, *113*, 9155.
[40] E. R. Lippincott, R. D. Nelson, *Spectrochim. Acta* **1958**, *10*, 307.
[41] D. Hartley, M. J. Ware, *J. Chem. Soc. A* **1969**, pp. 138.
[42] This degree of agreement is typical for the DFT level employed; see for example ref. [5].
[43] J. R. Cheeseman, G. W. Trucks, T. A. Keith, M. J. Frisch, *J. Chem. Phys.* **1996**, *104*, 5497.
[44] *Gaussian98* (revision A.7), M. J. Frisch, G. W. Trucks, H. B. Schlegel, G. E. Scuseria, M. A. Robb, J. R. Cheeseman, V. G. Zakrzewski, J. A. Montgomery, R. E. Stratman, J. C. Burant, S. Dapprich, J. M. Milliam, A. D. Daniels, K. N. Kudin, M. C. Strain, O. Farkas, J. Tomasi, V. Barone, M.Cossi, R.Cammi, B. Mennucci, C. Pomelli, C. Adamo, S. Clifford, J. Ochterski, G. A. Petersson, P. Y. Ayala, Q.

Cui, K. Morokuma, D. K. Malick, A. D. Rabuck, K. Raghavachari, J. B. Foresman, J. Cioslowski, J. V. Ortiz, A. G. Baboul, B. B. Stefanov, C. Liu, A. Liashenko, P. Piskorz, I. Komaromi, R. Gomperts, R. L. Martin, D. J. Fox, T. Keith, M. A. Al-Laham, C. Y. Peng, A. Nanayakkara, C. Gonzalez, M. Challacombe, P. M. W. Gill, B. G. J. W. Chen, M. W. Wong, J. L. Andres, M. Head-Gordon, E. S. Replogle, J. A. Pople, Gaussian, Inc., Pittsburgh PA, **1998**.
[45] A. D. Becke, *J. Chem. Phys.* **1993**, *98*, 5648.
[46] C. Lee, W. Yang, R. G. Parr, *Phys. Rev. B* **1988**, *37*, 785.
[47] W. Kutzelnigg, U. Fleischer, M. Schindler, *NMR* **1990**, *23*, 165.
[48] CPMD Version 3.3a, J. Hutter, A. Alavi, T. Deutsch, M. Bernasconi, S. Goedecker, D. Marx, M. Tuckermann, M. Parrinello, Max-Planck-Institut für Festkörperforschung (Stuttgart) and IBM Research Laboratory (Zürich), **1995–1999**.
[49] N. Troullier, J. L. Martins, *Phys. Rev. B* **1991**, *43*, 1993.
[50] L. Kleinman, D. M. Bylander, *Phys. Rev. Lett.* **1982**, *48*, 1425.
[51] Dalton, a molecular electronic structure program, release 1.2, T. Helgaker, H. J. A. Jensen, P. Jørgenson, J. Olsen, K. Ruud, H. A. gren, A. A. Auer, K. L. Bak, V. Bakken, O.Christiansen, S. Coriani, P.Dahle, E. K. Dalskov, T. Enevoldsen, B. Fernandez, C. Hättig, K. Hald, A.Halkier, H. Heiberg, H. Hettema, D. Jonsson, S. Kirpekar, R. Kobayashi, H. Koch, K. V. Mikkelsen, P. Norman, M. J. Packer, T. B. Pedersen, T. A. Ruden, A. Sanchez, T. Saue, S. P. A. Sauer, B. Schimmelpfennig, K. O. Sylvester-Hvid, P. R. Taylor, O. Vahtras, **2001**.
[52] Y. Morino, H. Uehara, *J. Chem. Phys.* **1966**, *45*, 4543.
[53] P. Briant, J. Green, A. Haaland, A. Møllendal, K. Rypdal, J. Tremmel, *J. Am. Chem. Soc.* **1989**, *111*, 3434.
[54] G. S. McGrady, A. J. Downs, D. C. McKean, A. Haaland, W. Scherer, H. P. Verne, H. V. Volden, *Inorg. Chem.* **1996**, *35*, 4713.
[55] K. Karakida, K. Kuchitsu, *Inorg. Chim. Acta* **1975**, *13*, 113.
[56] H. Oberhammer, J. Strähle, *Z. Naturforsch.* **1975**, *30a*, 296.
[57] A. Almenningen, S. Samdal, D. Christen, *J. Mol. Struct.* **1978**, *48*, 69.
[58] K. Hagen, M. M. Gilbert, L. Hedberg, K. Hedberg, *Inorg. Chem.* **1982**, *21*, 2690.
[59] S. J. L. Placa, W. C. Hamilton, J. A. Ibers, A. Davison, *Inorg. Chem.* **1969**, *8*, 1928.
[60] B. Beagley, D. Schmidling, *J. Mol. Struct.* **1974**, *22*, 466.
[61] M. Davies, C. Speed, *J. Organomet. Chem.* **1970**, *21*, 401.
[62] R. Bohn, A. Haaland, *J. Organomet. Chem.* **1966**, *5*, 470.
[63] V. V. Tkachev, L. O. Atovmyan, *Zh. Strukt. Khim.* **1972**, *13*, 287.
[64] A. Clearfield, D. K. Warner, C. H. Saldarriaga-Molina, R. Ropal, I. Bernal, *Can. J. Chem.* **1975**, *53*, 1622.
[65] J. Ellis, K. M. Chi, *J. Am. Chem. Soc.* **1990**, *112*, 6022.
[66] B. A. Frenz, J. A. Ibers, *Inorg. Chem.* **1972**, *11*, 1109.
[67] J. Cowie, E. J. M. Hamilton, J. C. V. Laurie, A. J. Welch, *J. Organomet. Chem.* **1990**, *394*, 1.
[68] P. T. Greene, R. F. Bryan, *J. Chem. Soc. A* **1971**, 1559.
[69] G. Doyle, K. A. Eriksen, D. V. Engen, *Organometallics* **1985**, *4*, 2201.
[70] Consistent with this observation, a static geometry optimization imposing C_{4v} symmetry and a C_{ax}-Ti-C_{eq} angle of 100° affords Ti–C_{ax} distances of 2.083 and 2.032 Å, the average of which is 0.002 Å shorter than the equilibrium value in Table 2.
[71] M. Bühl, R. Schurhammer, P. Imhof, *J. Am. Chem. Soc.* **2004**, *126*, 3310.
[72] M. Bühl, F. T. Mauschick, B. Wrackmeyer, *Angew. Chem.* **2002**, *114*, 2421; *Angew. Chem. Int. Ed.* **2002**, *41*, 2312.
[73] M. Toyama, T. Oka, Y. Morino, *J. Molec. Spectrosc.* **1964**, *13*, 193.
[74] T. A. Ruden, K. Ruud in *Calculation of NMR and EPR Parameters. Theory and Applications* (Eds.: M. Kaupp, M. Bühl, V. G. Malkin), Wiley-VCH, Weinheim, **2004**, pp. 421.
[75] Preliminary results for selected examples from our study indeed indicate that also for transition-metal compounds, quantum thermal effects tend to be smaller than zero-point corrections.
[76] W. Leitner, M. Bühl, R. Fornika, C. Six, W. Baumann, E. Dinjus, M. Kessler, C. Kruger, A. Rufinska, *Organometallics* **1999**, *18*, 1196.
[77] J. G. Donkervoort, M. Bühl, J. M. Ernsting, C. J. Elsevier, *Eur. J. Inorg. Chem.* **1999**, 27.
[78] C. J. Jameson, D. Rehder, M. Hoch, *J. Am. Chem. Soc.* **1987**, *109*, 2589.
[79] N. Godbout, E. Oldfield, *J. Am. Chem. Soc.* **1997**, *119*, 8065.
[80] See for example: G. Schreckenbach, *J. Chem. Phys.* **1999**, *110*, 11936.
[81] This term contains also an additional, similar matrix element with an r^{-3} operator, which we have omitted since it does not alter any of the following qualitative discussions.
[82] See for example: G. Schreckenbach, T. Ziegler, *J. Phys. Chem.* **1995**, *99*, 606.
[83] J. G. Palenik, *Inorg. Chem.* **1967**, *6*, 503.
[84] N. Hao, B. G. Sayer, G. Denes, D. G. Bickley, C. Detellier, M. J. McGlinchey, *J. Magn. Reson.* **1982**, *50*, 50.
[85] S. Berger, W. Bock, G. Frenking, V. Jonas, V. Müller, *J. Am. Chem. Soc.* **1995**, *117*, 3820.
[86] F. J. Feher, R. L. Blanski, *Organometallics* **1993**, *12*, 958.
[87] B. Wrackmeyer, T. Hofmann, M. Herberhold, *J. Organomet. Chem.* **1995**, *486*, 255.
[88] M. Koller PhD thesis, University Zürich, **1993**.
[89] E. J. Meier, W. Kozminski, A. Linden, P. Lustenberger, W. v. Philipsborn, *Organometallics* **1996**, *15*, 2469.

Received: March 16, 2004
Published online: September 27, 2004